JOURNAL OF CATALYSIS 147, 515–524 (1994)

The Role of Co in Unsupported Co–Mo Sulfides in the Hydrodesulfurization of Thiophene

Kazuhiro Inamura[1] and Roel Prins

Laboratorium für Technische Chemie, Eidgenössische Technische Hochschule, 8092 Zürich, Switzerland

Received June 9, 1993; revised December 10, 1993

Unsupported Co–Mo catalysts were prepared by impregnation of MoS_2, obtained by thermal decomposition of ammonium tetrathiomolybdate, with a solution of cobalt nitrate in acetone. XRD and HREM showed that the MoS_2 structure of the resulting catalysts remained intact upon addition of Co. The thiophene hydrodesulfurization and the consecutive butene hydrogenation properties indicated that the Co ions are preferentially situated at the edges of the MoS_2 crystallites below Co/(Co + Mo) = 0.08 and promote the hydrodesulfurization (HDS) reaction. Further addition of Co leads to the segregation of Co_9S_8, which acts as a support for highly dispersed Co-promoted MoS_2 crystallites. As a result of this structural effect, the Co–MoS_2 crystallites become better accessible and the catalytic activity increases again above Co/(Co + Mo) = 0.2. The observed increase in activity upon physical mixing of Co-promoted MoS_2 and Co_9S_8 might also be explained by such a structural effect, rather than by a remote-control effect.

INTRODUCTION

To explain the role of the Co (or Ni) promoter in Co–Mo (or Ni–Mo) hydrodesulfurization (HDS) catalysts several studies have been performed on unsupported promoted MoS_2 catalysts. However, unsupported sulfides have much less surface area than supported catalysts and therefore methods for preparing highly dispersed unsupported sulfides have been developed. The homogeneous sulfide precipitation (HSP) method (1) was reported to give a better dispersion of both the Co and Mo atoms than the co-maceration (2, 3) and oxide precipitation (4) methods. In the impregnated thiosalt decomposition method, Co^{2+} ions are impregnated on ammonium tetrathiomolybdate [$(NH_4)_2MoS_4$] crystals and the resulting system is subsequently sulfided (5, 6). However, the morphology and catalytic activity of the resulting catalysts were not much improved compared to those of the corresponding HSP catalyst, probably because a large fraction of the Co ions was occluded by the MoS_2 crystals during the decomposition of the $(NH_4)_2MoS_4$ precursor, just as in the other preparation methods. Recently, Halbert *et al.* achieved a selective decoration of the MoS_2 edges by promoter atoms via reaction of MoS_2 with $Co_2(CO)_8$ (7).

In this work we prepared unsupported Co–Mo sulfide catalysts by impregnating Co^{2+} ions on MoS_2, which was obtained by presulfiding of $(NH_4)_2MoS_4$. The resulting sulfide catalysts should provide us with a clear picture of the role of Co in unsupported Co–Mo sulfides, because the physical properties of the MoS_2 support are expected to stay constant during the Co-addition treatment. For comparison, another set of sulfide catalysts was prepared by the HSP method. The catalytic activity and the catalyst structure of both types of catalyst were studied as a function of the Co content by means of thiophene hydrodesulfurization, X-ray diffraction, and high-resolution electron microscopy.

EXPERIMENTAL

Pure cobalt sulfide was prepared by treating cobalt acetate (Aldrich) in flowing He at 393 K for 2 h, and then in a flow of 10% H_2S/H_2 at 393 K for 1 h. Subsequently the temperature was raised at 2 K min^{-1} to 673 K, and kept at this level for 2 h. The sample was then purged at 673 K and cooled to room temperature in flowing He. Pure MoS_2 was obtained by thermal decomposition of $(NH_4)_2MoS_4$, prepared as described in Ref. (8), at 673 K for 2 h, using the same treatment as in the preparation of pure cobalt sulfide. Cobalt-containing MoS_2 samples were prepared by impregnation of pure MoS_2 with a solution of $Co(NO_3)_2 \cdot 6H_2O$ (Johnson Matthey, 99%) in acetone. The suspension was refluxed under stirring at 325 K for 5 h under N_2 and then evaporated to dryness. Subsequently, the sample was sulfided at 673 K for 2 h as described above. The resulting catalysts are denoted Co(x)/SATM, where x is the Co/(Co + Mo) atomic ratio and SATM indicates that MoS_2 obtained from sulfided ammonium tetrathiomolybdate is used as the support. Another set of samples obtained by the homogeneous sulfide precipitation (HSP) method was prepared by the

[1] To whom correspondence should be addressed at present address: Central Research Laboratories, Idemitsu Kosan Co., Ltd., 1280 Kamiizumi, Sodegaura, Chiba 299-02, Japan.

0021-9517/94 $6.00

method described by Hoodless *et al.* (9). The black precursor precipitates were sulfided at 673 K for 2 h, as described above. This series of catalysts is denoted Co(x)-HSP. All sulfided samples were exposed to air at room temperature and stored in a vacuum desiccator before use.

The hydrodesulfurization of thiophene was studied in a flow system with a microreactor operating at atmospheric pressure. Sulfided samples of ca. 0.2 g were resulfided in a flow of 60 cm^3 min^{-1} of 10% H_2S/H_2 while the temperature was raised at 6 K min^{-1} to 673 K, kept at this temperature for 1 h, and then cooled to 593 K. Thereafter a gas mixture of 3% thiophene (Merck p.a.) in H_2 was introduced at a flow of 60 cm^3 min^{-1}. The reaction rate constant for hydrodesulfurization (HDS) and hydrogenation (HYD) were calculated using the mean conversions measured after 2 and 3 h reaction time, and assuming first-order reaction in thiophene hydrodesulfurization and in the consecutive butene hydrogenation (10). Steady-state sulfide catalysts were prepared by reacting at 593 K for 6 h, cooling under H_2 to room temperature, and storing in a vacuum desiccator.

Surface areas of the freshly sulfided and steady-state catalysts were determined by N_2 adsorption on a Micromeritics ASAP 2000M instrument. X-ray diffraction (XRD) data of the freshly sulfided samples were collected on a Siemens D5000 diffractometer (Cu Kα, 40 kV, 30 mA) with a step length of 0.02° (2θ). It was checked that the XRD patterns of the freshly sulfided MoS_2 (at 673 K) remained unchanged during the HDS reaction (at 593 K). Peak decomposition was carried out by means of profile fitting with a pseudo-Voigt function. Examples of calculated line profiles are shown in Fig. 2. The average crystallite sizes of MoS_2, in the MoS_2 plane of the layers (L_a) and perpendicular to the plane (L_c), were determined from the broadening of the (10x) reflection, which consists of the overlapping (100) and (101) reflections, and the (002) reflection respectively, with the Scherrer equation using K values of 2.0 for L_a and 0.9 for L_c (11). The line broadening $\delta(2\theta)$, defined as the full width at half-maximum intensity (FWHM), was corrected by the instrumental resolution.

High-resolution electron microscopy (HREM) was carried out by grinding the sulfided samples to a fine powder, suspending the powder in heptane, dispersing it by ultrasonic treatment for 5 min, and then drying on holey carbon films supported on copper grids. The mesurements were made on a Hitachi H-800 electron microscope operated at 200 kV.

RESULTS

The BET surface areas of the sulfide catalysts measured before and after the HDS reaction are listed in Table 1. The surface areas of both series of catalyst are affected by the Co contents, which indicates that the Co content influences the morphology and/or the degree of aggregation of the Co–Mo sulfide phases. The surface areas of the Co(x)/SATM catalysts are generally lower than those of the corresponding Co(x)-HSP catalysts.

TABLE 1

Surface Areas of the Fresh and the Steady-State Sulfide Catalysts

Catalyst	Co/(Co + Mo)	Surface area/m^2 g^{-1}	
		Fresh	Steady-state
Co(0.0)-HSP	0.000	75	26
Co(0.1)-HSP	0.103	52	52
Co(0.2)-HSP	0.201	16	—
Co(0.3)-HSP	0.299	26	—
Co(0.5)-HSP	0.500	48	—
Co(0.7)-HSP	0.700	43	43
Co(0.0)/SATM	0.000	37 ± 7[a]	13 ± 1[a]
Co(0.1)/SATM	0.100	24	12
Co(0.2)/SATM	0.198	20	19
Co(0.3)/SATM	0.300	30 ± 4[a]	26 ± 3[a]
Co(0.5)/SATM	0.504	40	23
Co(0.63)/SATM	0.627	29	30
Co sulfide	1.000	21	18

[a] Mean value of three different samples with standard deviation.

The XRD patterns of the Co(x)-HSP catalysts are given in Fig. 1. Below x = 0.3 they are composed of diffractions of poorly crystalline MoS_2 only, indicating that the MoS_2 keeps its structure in the presence of Co, and that the Co is present as an "X-ray amorphous" phase, as reported before by Candia *et al.* (1). Above x = 0.5, bulk Co sulfide phases appear superimposed on the MoS_2 phase. Co_9S_8 is present in the x = 0.5 and x = 0.7 catalysts and CoS_{1+x} is somewhat present in the x = 0.7 catalyst. The CoS_{1+x} phase is assigned to $CoS_{1.097}$ (JCPDS 19-366).

The XRD patterns of the Co(x)/SATM catalysts and that of pure Co sulfide obtained from cobalt acetate are shown in Fig. 2. The XRD pattern of sulfided $(NH_4)_2MoS_4$ is almost identical with that of Co(0.0)-HSP. Distinct from the HSP catalysts, Co_9S_8 is already present in the SATM catalysts at x = 0.2, and may be even at x = 0.1. The Co_9S_8 phase becomes dominant with increasing Co/(Co + Mo) ratio, and is finally the only phase present in the pure Co sulfide catalyst.

The average MoS_2 crystallite sizes were estimated from the XRD data. As shown in Fig. 3, the MoS_2 crystallite sizes of the Co(x)-HSP catalysts gradually decrease from 87 to 62 Å for L_a, and from 33 to 21 Å for L_c when x increases from 0 to 0.5. At the same time the average number of layers (L_c/6.15 Å) in the Co(x)-HSP catalysts

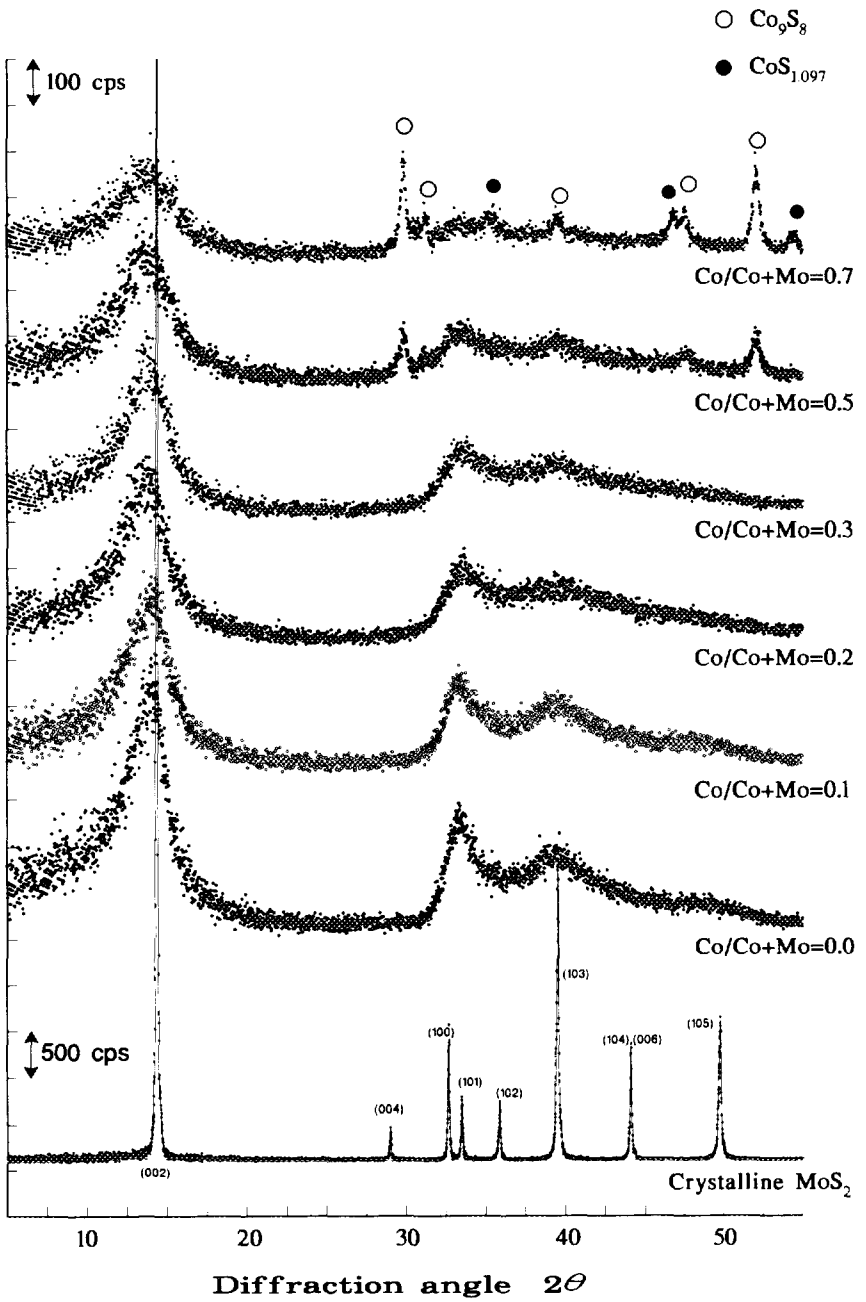

FIG. 1. XRD patterns of Co(x)-HSP catalysts and of well-crytallized MoS_2 (labeled on the basis of the 2H-MoS_2 structural data, (JCPDS 37-1492).

decreases from 5.3 to 3.3, in agreement with results reported for Co–Mo- (1) and Ni–Mo-HSP catalysts (12).

The Co(0.0)/SATM catalyst shows almost the same crystallite sizes as the Co(0.0)-HSP catalyst. The most remarkable feature of the Co(x)/SATM catalysts is the constancy of the MoS_2 crytallite sizes in the Co/(Co + Mo) range between 0 and 0.4 (Fig. 3, upper panel). This indicates that the MoS_2 structure acts as a support for the Co during the Co addition, and does not undergo a reconstruction. Beyond $x = 0.4$, the L_c value seems to decrease, while no conclusion can be drawn about the L_a value of Co(x)/SATM catalysts, because of the hardly discernible (10x) peak. The average crystallite size of the Co_9S_8 phase, which was determined from the FWHM of the (311) reflection using a K value of 0.9, was in the 270–400 Å range for Co(x)/SATM catalysts with $x \geq 0.3$, as well as for the pure Co sulfide.

HREM images of some Co(x)-HSP catalysts are shown

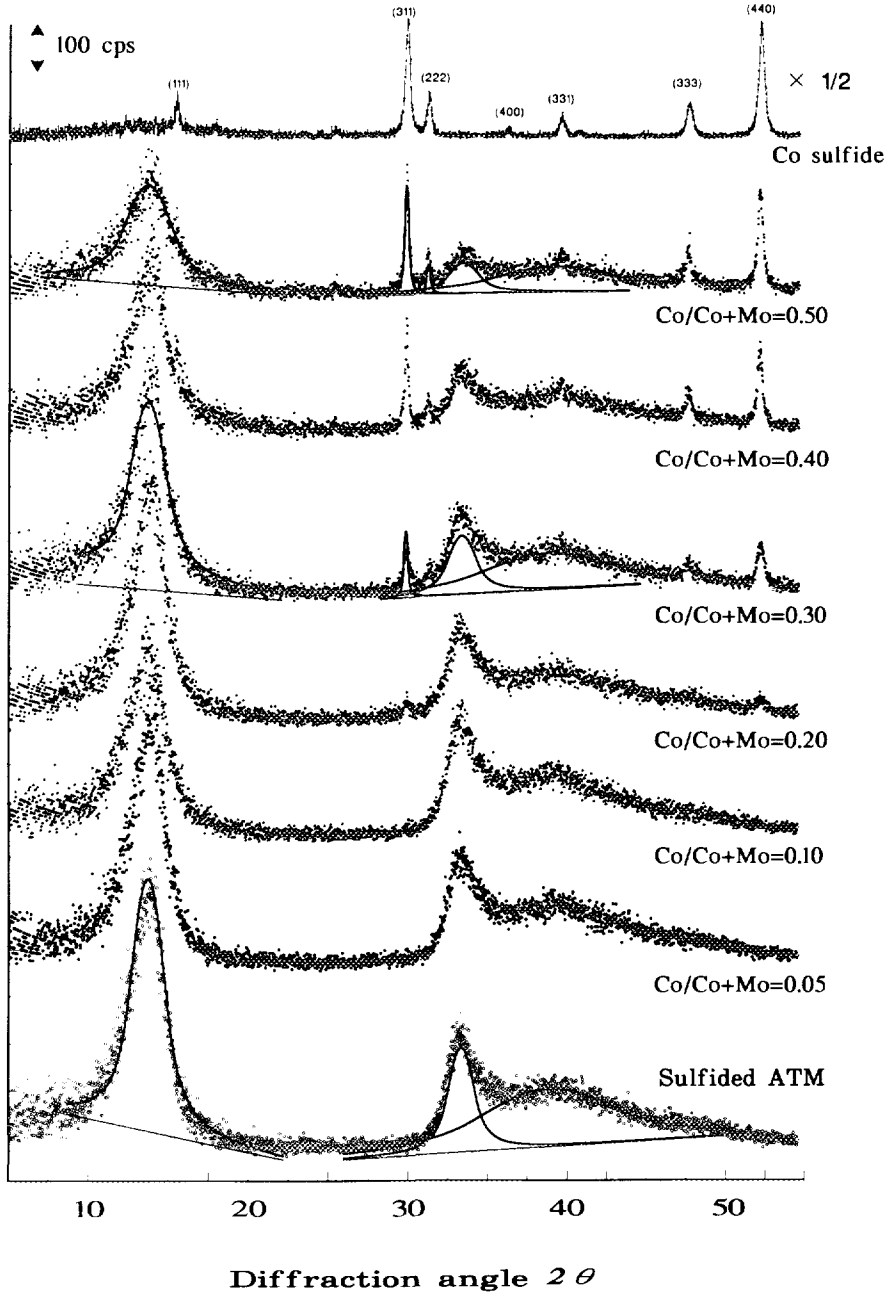

FIG. 2. XRD patterns of Co(x)/SATM catalysts and of pure Co sulfide (labeled on the basis of the Co_9S_8 structural data, JCPDS 19-364).

in Fig. 4. In all micrographs of Mo-containing samples, MoS_2 crystallites can be clearly seen in the form of groups of parallel dark lines, separated by a 6.2 Å spacing of the (002) 2*H*-MoS_2 planes. In the HREM of Co(0.0)-HSP (Fig. 4a), the number of MoS_2 layers of the MoS_2 crystallites seems to range from 4 to 8 with an average value of 5–6, consistent with the value of 5.3 estimated by XRD. Many MoS_2 crystallites larger than 100 Å can be seen in the HREM of Co(0.0)-HSP, despite the XRD estimate of 87 Å (Fig. 3). One explanation of this discrepancy could be the presence of crystallite defects along the direction of the MoS_2 layers which reveal themselves in the HREM images as winding and bending structures, and which would reduce the L_a value determined by XRD.

In the HREM images of the Co(x)-HSP catalysts with $x > 0.5$, regular straight lines are identified in addition to the MoS_2 stacks (cf. Fig. 4c). These planes are also observed in the HREM images of the pure Co sulfide in Fig. 4d, and are undoubtedly due to cubic Co_9S_8 crystallites (6, 13). Some MoS_2 stacks are situated with their basal

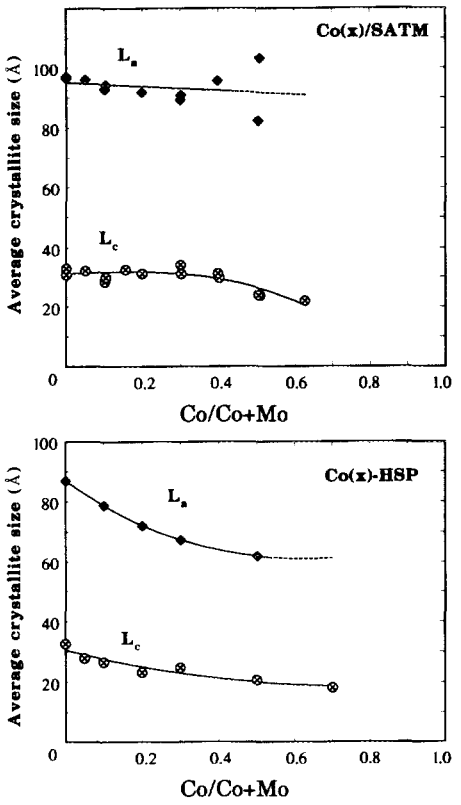

FIG. 3. Crystallite size of MoS_2 in the plane of the MoS_2 layers L_a (◆) and perpendicular to the plane L_c (⊗) versus the Co/Co + Mo atomic ratio for Co(x)-HSP and Co(x)/SATM catalysts.

planes parallel to the contour of the Co_9S_8 crystallites. In this case the layered MoS_2 structures appear to be 2–5 layers high and lower than those of the Co(0.0)- and Co(0.3)-HSP catalysts. This micrograph is reminiscent of HREM images of MoS_2 supported on an oxide support such as alumina, silica, or titania (14,15). This morphological similarity suggests that bulk Co sulfide serves as a carrier for well-dispered MoS_2 stacks (4, 16–18).

In accordance with the similarity of the XRD patterns of Co(0.0)/SATM and Co(0.0)-HSP, the HREM image of Co(0.0)/SATM in Fig. 5a is similar to that of Co(0.0)-HSP with respect to the stacking of the MoS_2 layers. In accordance with the early detection of Co_9S_8 phases by XRD, square-shaped planes of cubic Co_9S_8 as well as randomly oriented MoS_2 stacks are already discernible in the HREM of Co(0.2)/SATM in Fig. 5b. As expected, an increase of the Co loading results in more Co_9S_8 crystallites, as shown in Figs. 5c and 5d. Also in these figures one observes that the MoS_2 stacks are located ("supported") on the surface of the Co_9S_8 crystallites, just as in Fig. 4c of the Co(0.7)-HSP sample.

The rate constant k_{HDS} and the ratio k_{HYD}/k_{HDS} are plotted in Fig. 6 as a function of the Co/(Co + Mo) = x atomic ratio. A typical synergistic promotional behavior is observed for the Co(x)/SATM catalysts, with a maximum HDS activity around x = 0.3–0.4, whereas an activity curve with two maxima seems to be present in the Co(x)-HSP catalysts. The HDS activity k_{HDS} of a Co(x)-HSP catalyst is generally higher than that of the corresponding Co(x)/SATM catalysts. However, this may partly be due to a difference in surface area. If k_{HDS} is recalculated by normalization to the steady-state surface area instead of to the catalyst weight, the HDS activity k_{HDS} of the Co(0.0)-HSP catalyst is nearly equal to that of the Co(0.0)/SATM catalyst, and the activity of the Co(x)-HSP catalysts shows a maximum at x = 0.2. The k_{HYD}/k_{HDS} ratio of both catalyst types decreases with increasing Co/(Co + Mo) atomic ratio. Although the ratios were determined at different conversion levels and thus at different H_2S concentrations, the observed decrease in k_{HYD}/k_{HDS} with increasing Co/(Co + Mo) ratio cannot be explained by an increased HDS conversion, because it is generally accepted that H_2S has little or no effect on the hydrogenation function, but depresses the hydrodesulfurization function (19). Thus, k_{HYD}/k_{HDS} will be enhanced rather than lowered at higher conversion (3), and the observed decrease in the k_{HYD}/k_{HDS} ratio must be due to a direct effect of Co.

DISCUSSION

Catalyst Morphology

The addition of Co to the HSP catalysts not only changed the catalytic activity, but also the dispersion and the morphology of MoS_2, as also observed in previous studies (1, 3, 4). These changes can be clearly seen from the average crystallite sizes of MoS_2 (Fig. 3) and the HREM images (Fig. 4), even at a Co/(Co + Mo) atomic ratio smaller than 0.3, where no bulk Co sulfide phase was detected by XRD. This makes it difficult to determine the role of Co in unsupported HSP catalysts, since not only a chemical (edge decoration) but also a structural (textural or morphological) promoting effect is involved.

In the Co(x)/SATM catalysts, on the other hand, the average crystallite sizes are maintained at least up to x = 0.4 (Fig. 3). As a consequence, a much smaller influence of the texture and/or morphology of the starting MoS_2 is to be expected in Co(x)/SATM catalysts. Assuming that all MoS_2 crystallites have the same regular hexagonal shape, with crystallite sizes L_a = 93 Å and L_c = 31 Å, equal to the average values determined for the Co(0.0–0.4)/SATM catalysts (Fig. 3), the geometrical surface area of the MoS_2 crystallites is calculated to be 224 $m^2\ g^{-1}$ (at a bulk MoS_2 density of 4.8 $g\ cm^{-3}$). This surface area is much higher than those measured for the Co(x)/SATM catalysts (20–40 $m^2\ g^{-1}$). Such a large difference between calculated and measured surface areas can only be due to the aggregation

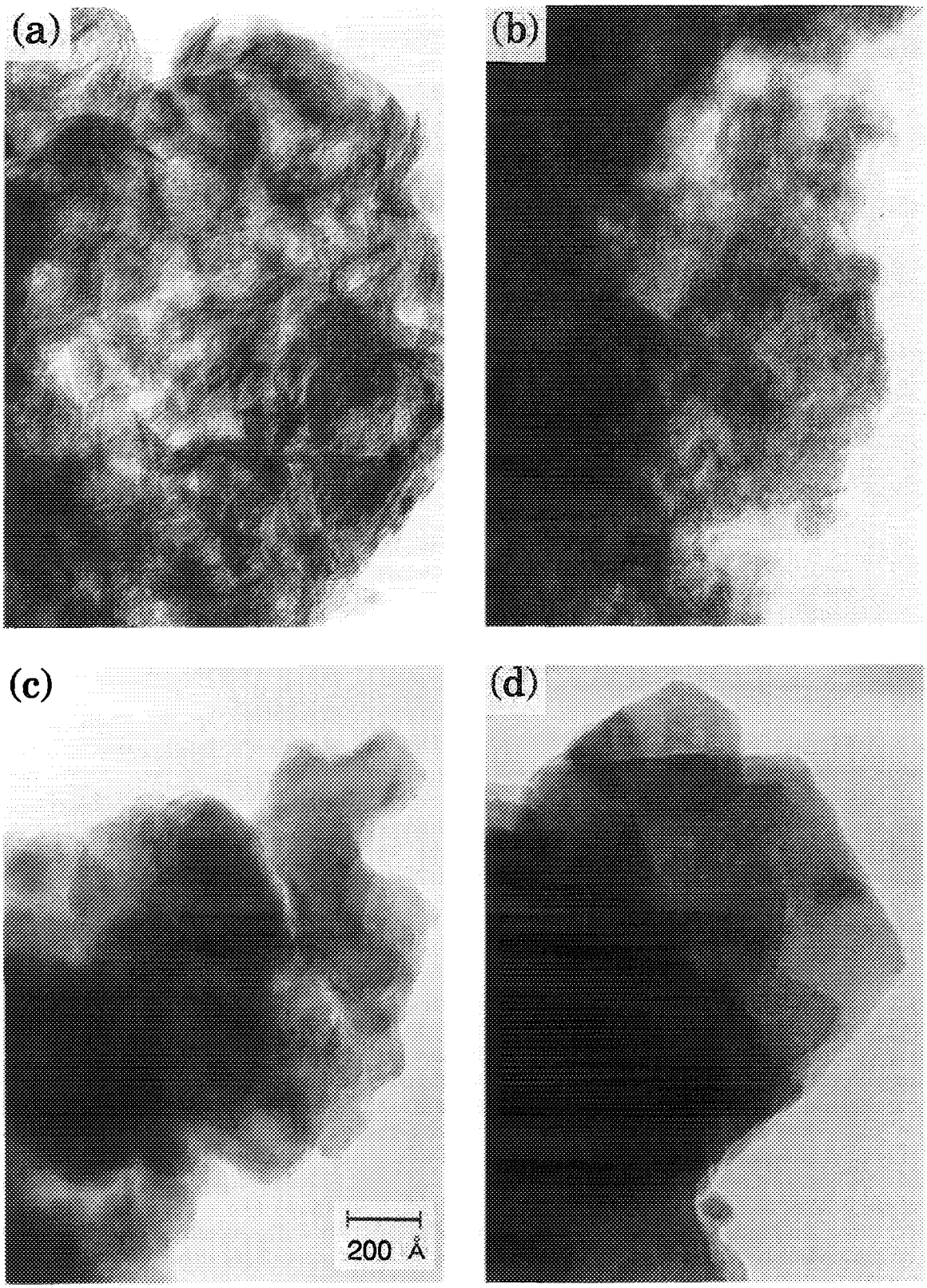

FIG. 4. High-resolution transmission electron micrographs of Co(x)-HSP and Co sulfide catalysts: (a) Co(0.0)-HSP, (b) Co(0.3)-HSP, (c) Co(0.7)-HSP, and (d) Co sulfide.

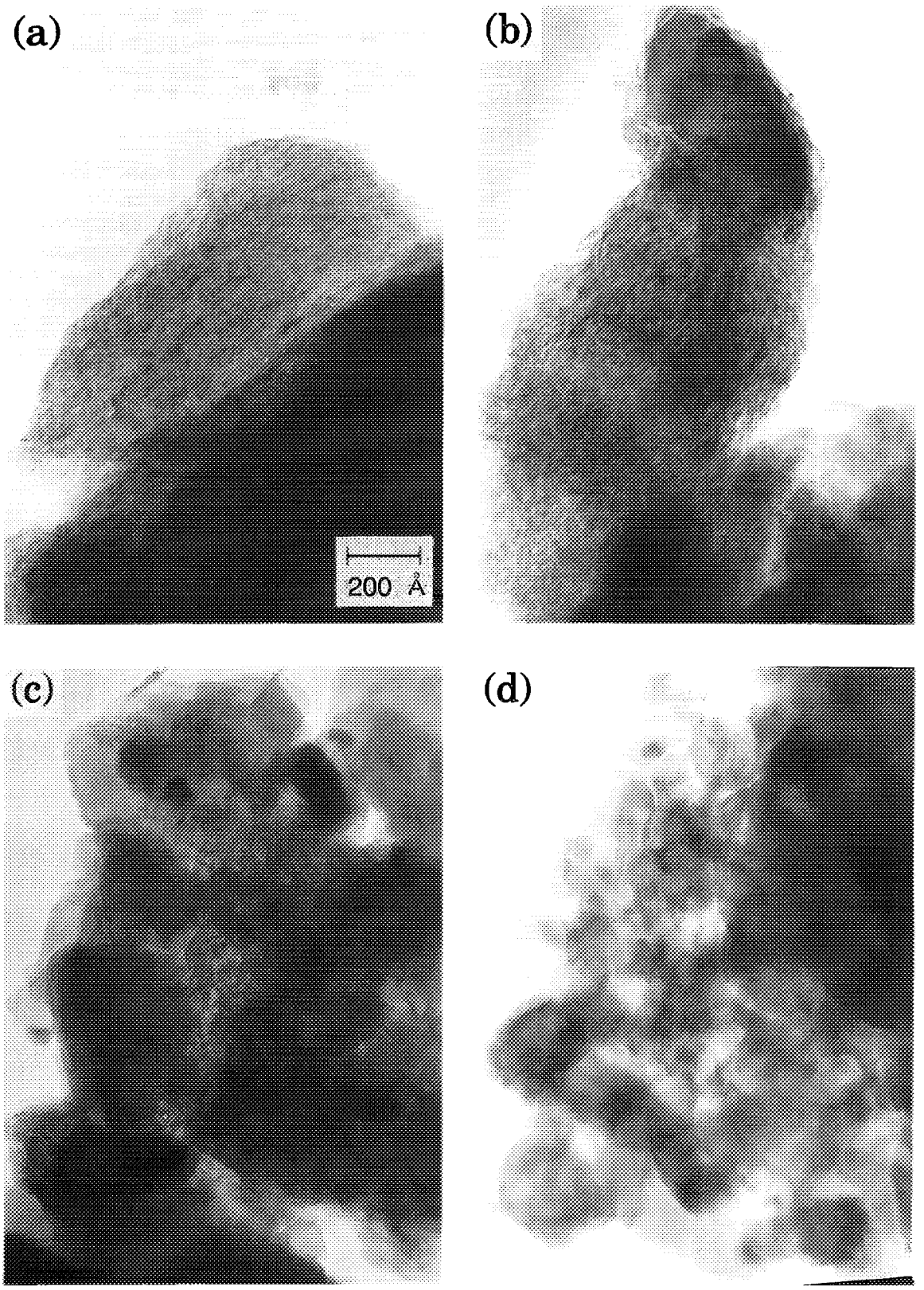

FIG. 5. High-resolution transmission electron micrographs of Co(x)/SATM catalysts: (a) Co(0.0)/SATM, (b) Co(0.2)/SATM, (c) Co(0.5)/SATM, and (d) Co(0.63)/SATM.

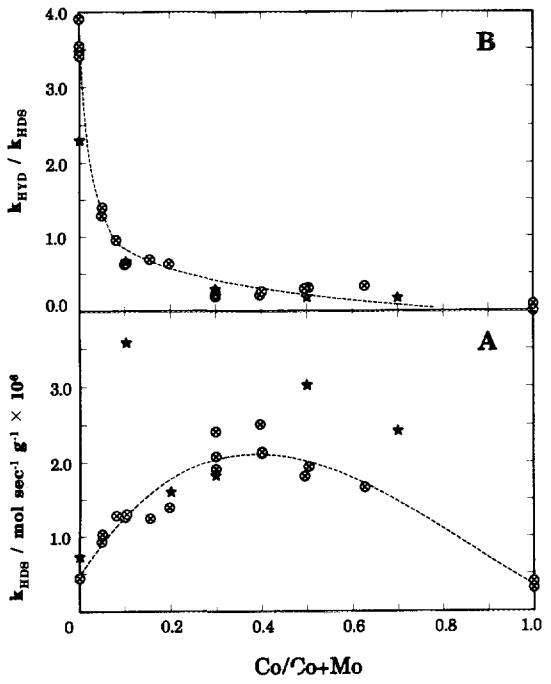

FIG. 6. The steady-state kinetic rate constant k_{HDS} (A) and the ratio k_{HYD}/k_{HDS} (B) at 593 K versus the Co/(Co + Mo) atomic ratio, for Co(x)/SATM (⊗), and Co(x)-HSP (*) catalysts.

of the MoS_2 crystallites, which form face-to-face and/or edge-to-face contacts, as seen in the HREM images shown in Fig. 5. Assuming that the structure of the MoS_2 crystallites is the same as that of bulk MoS_2 (with Mo ions in the centers of trigonal prismatic units of six S ions, and with a Mo–Mo distance of 3.16 Å), each MoS_2 crystallite has $n = 18$ Mo ions along every hexagonal edge and contains $k = 5$ stacked MoS_2 layers. According to the model presented by Kasztelan *et al.* (20), these crystallites thus consist of $(3n^2 - 3n + 1) \times k = 4595$ Mo ions ($[Mo]_{total}$), $(6n - 12) \times k = 480$ edge Mo ions ($[Mo]_{edge}$), and $6 \times k = 30$ corner Mo ions ($[Mo]_{corner}$).

The Co promoter ions are located along the edges of MoS_2 (21, 22). Extended X-ray absorption fine structure investigations have shown that the most likely position for the promoter ions in sulfided Co–Mo, Ni–Mo, and Ni–W catalysts is a square pyramidal site (23, 24, 10). The number of available square pyramidal sites along the MoS_2 edges depends on the number of edge Mo ions, and on the types of edge planes, while this site is only possible on the $(10\bar{1}0)$ edge, unless a reconstruction of the $(\bar{1}010)$ edge plane takes place (24). Regardless of whether a reconstruction takes place or not, it is hard to imagine that all available square pyramidal sites are occupied by Co ions. In such a case all Co ions would be positioned on neighboring sites, which is expected to bring about a large rearrangement of the edge S ions (24). Therefore, the number of Co atoms at the MoS_2 edges in our Co(x)/SATM catalysts should be smaller than the total number of Mo edge ions, so that the $[Co]_{edge}/([Co]_{edge} + [Mo]_{total})$ ratio is expected to be 0.10 at most.

The Role of Co

The plot of k_{HDS} (mol s^{-1} (g cat)$^{-1}$) against x for Co(x)/SATM catalysts (Fig. 6A) can be converted into a k''_{HDS} (mol s^{-1} (g MoS_2)$^{-1}$) plot by normalization to the MoS_2 content instead of to the catalyst weight, as shown in Fig. 7A. Although the reproducibility of k''_{HDS} around $x = 0.3$ is not very good, the k''_{HDS} plot can be divided into four regions and interpreted as follows.

The k''_{HDS} increases with increasing x in the low-Co-content region ($0 < x < 0.08$), and then stays constant

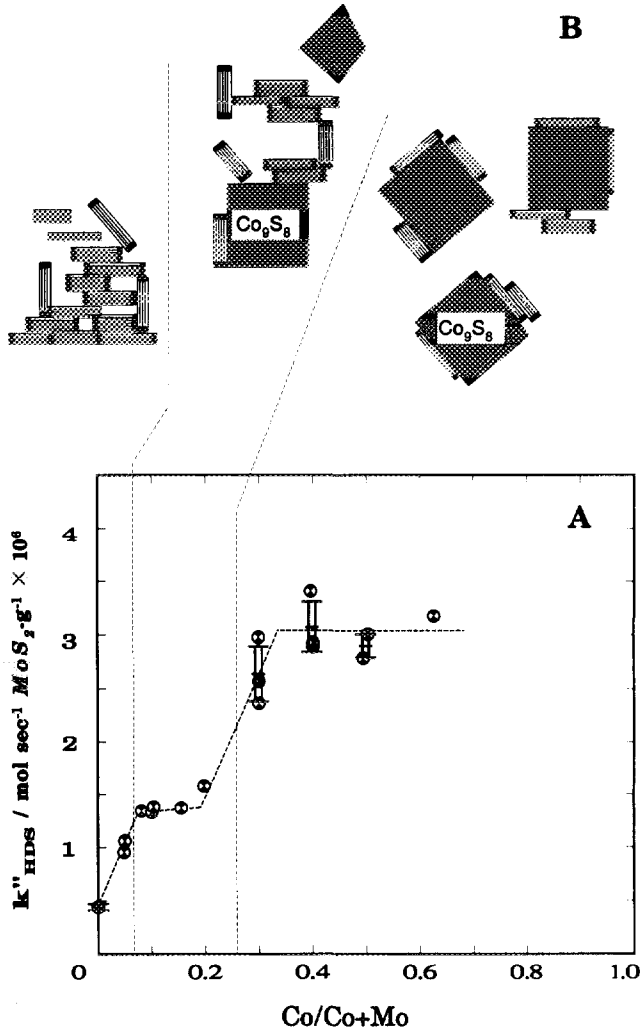

FIG. 7. (A) The rate constant k''_{HDS} normalized to the MoS_2 content versus the Co/(Co + Mo) atomic ratio for Co(x)/SATM catalysts, with standard deviations given by error bars. (B) Schematic models for the Co sulfide and the MoS_2 crystallite phases.

up to $x = 0.2$. The promoting effect, defined as the ratio of the rate constant for the promoted catalyst to that for the unpromoted catalyst, is ca. 3 at this first plateau. Subsequently, k''_{HDS} increases again and finally reaches another constant level in the $x = 0.4$–0.6 range, with a promoting effect of about 7. The first increase in k''_{HDS} up to $x = 0.08$ may be attributed to the decoration of the MoS_2 edges by the Co ions. The first saturating point at $x = 0.08$ is in good agreement with the estimated maximum $[Co]_{edge}/([Co]_{edge} + [Mo]_{total})$ ratio. The promoting effect in this range is about 3, similar to the value of 3.3 proposed by Halbert et al. (7) as the electronic promoting effect of Co for Co–Mo sulfide catalysts, prepared by reacting MoS_2 with $Co_2(CO)_8$, in the HDS of dibenzothiophene.

Since neither any further edge decoration, nor any significant structural changes in the MoS_2 crystallites is to be expected above $x = 0.2$, the explanation for the second promotion effect for $x > 0.2$ must be related to the formation of Co_9S_8 crystallites, as revealed by the XRD and HREM results. Two explanations can be given. One is that the bulk Co sulfide functions as a carrier for well-dispersed MoS_2 stacks as suggested by the HREM micrographs, and as schematically depicted in Fig. 7B. A similar model has been proposed before (7, 16, 25). The structural effect in unsupported HSP catalysts is difficult to determine, because the promoting Co ions can play a role not only in the edge-decoration effect, but also in the structural effect as a Co_9S_8 carrier for the MoS_2 crystallites. The combination of these two promoting effects may be highly dependent on the catalyst preparation procedure and may explain the variation in the optimum $M/(M + Mo)$ (M = Co, Ni) atomic ratios reported in the literature, ranging from 0.3 (3) to 0.54 (9) for Co–Mo sulfide catalysts, and from 0.55 (4) to 0.7 (12) for Ni–Mo sulfide catalysts. In our Co(x)/SATM catalysts, the Co addition may be moderate enough to maintain the morphology of the original MoS_2 crytallites in the low-Co-content region, so that the structural promoting effect is negligible. Further addition of Co induces the formation of Co_9S_8 crystallites and then the upper limit of the structural effect may be ca. $7/3 = 2.3$ in the $x = 0.4$–0.6 range. The unsupported catalyst might even have a higher activity if all individual MoS_2 crystallites were completely separated and effectively supported on the Co_9S_8 crystallites.

An alternative explanation for the second promotion effect would be the remote control model (26), in which it is postulated that a fraction of hydrogen dissociates on Co_9S_8 and spills over onto the surface of MoS_2, where it creates or maintains coordinatively unsaturated Mo sites as catalytically active sites. This could also explain the second increase in k''_{HDS} observed in our Co(x)/SATM catalysts in he $x > 0.2$ region, where Co-promoted MoS_2 crystallites coexist with Co_9S_8 crystallites. Taking the hydrogenation activity into consideration, however, we believe that the structural effect is the appropriate explanation, rather than the remote control effect. The high hydrogenation activity of alumina-supproted MoS_2 catalysts has been attributed to the edges of MoS_2 crytallites (27–29). The addition of Co ions to the edges of the MoS_2 crystallites would block coordinatively unsaturated Mo sites on the edges, and decrease the hydrogenation activity. This might explain the steep decrease in k_{HYD}/k_{HDS} of Co(x)/SATM catalysts with increasing Co/(Co + Mo) ratio in the low-Co-content region in Fig. 6B. If the remote control theory were valid, however, at low Co concentrations coordinatively unsaturated Mo sites would be present and consequently the promoted catalyst should show a high hydrogenation activity as well as a high hydrodesulfurization activity.

The structural promoting effect can also explain the curious synergy observed in mechanical mixtures of "CoMoS" and Co_9S_8 (30), and "NiMoS" and Co_9S_8 (31). Although a chemical interaction is not expected in such mechanical mixtures, it is probable that initially aggregated "CoMoS" (or "NiMoS") phases will be partially dispersed and supported on the Co_9S_8 (or Ni_3S_2) crystallites during the mixing and the subsequent sulfidation treatments. The observed increased activity after mixing can therefore be explained by an improvement in the accessibility of the CoMoS phase, instead of by remote control.

A similar double increase in activity for unsupported promoted sulfide catalysts as in Fig. 7 has been observed before by Farragher and Cossee in their study of the hydrogenation of benzene and cyclohexene by Ni-promoted WS_2 (32). Although they assumed the position of the Ni ions to be between WS_2 layers, rather than at the edge of the WS_2 layers in the W plane, they interpreted the first increase at low Ni/W atomic ratio to be due to the direct promoting effect of Ni. The second increase in hydrogenation activity at somewhat higher Ni/W ratio was not explained, although it was noted that it coincided with the first visibility in XRD of Ni_3S_2. In our interpretation, this second increase is caused by a better dispersion of the WS_2 layers by the interjacent Ni_3S_2 particles.

The present work demonstrates that one should be careful in using unsupported catalysts as model systems. Although they have in principle the advantage of simplicity, since, for instance, no support influences need to be considered, they have the disadvantage that part of their surface area is not accessible. As the present study has shown, this constitutes a huge problem when this accessibility is changed due to changes in the structure of the unsupported catalyst. In studies of unsupported catalyst in which one parameter or another is varied, such as

the Co/Mo ratio in the present case, it is thus of utmost importance to take the structure and texture of the resulting catalysts into account.

ACKNOWLEDGMENTS

We thank M. Ogishima (Idemitsu Kosan Co., Ltd.) for carrying out the HREM measurements. One of us (K.I.) acknowledges the financial support of the Japan Cooperation Center for Petroleum Industry Development (JCCP) and Idemitsu Kosan Co., Ltd., which enabled him to carry out this work.

REFERENCES

1. Candia, R., Clausen, B. S., and Topsøe, H., *Bull. Soc. Chim. Belg.* **90,** 1225 (1981).
2. Thakur, D. S., Grange, P., and Delmon, B., *J. Less Comm. Met.* **64,** 201 (1979).
3. Vrinat, M. L., and de Mourgues, L., *Appl. Catal.* **5,** 43 (1983).
4. Pratt, K. C., Sanders, J. V., and Tamp, N., *J. Catal.* **66,** 82 (1980).
5. Fuentes, S., Diaz, G., Pedraza, F., Rojas, H., and Rosas, N., *J. Catal.* **113,** 535 (1988).
6. Cruz-Reyes, J., Avalos-Borja, M., Farias, M. H., and Fuentes, S., *J. Catal.* **137,** 232 (1992).
7. Halbert, T. R., Ho, T. C., Stiefel, E. I., Chianelli, R. R., and Daage, M., *J. Catal.* **130,** 116 (1991).
8. McDonald, J. W., Friesen, D. G., Rosenheim, L. D., and Newton, W. E., *Inorg. Chim. Acta* **72,** 205 (1982).
9. Hoodless, R. C., Moyes, R. B., and Wells, P. B., *Bull. Soc. Chim. Belg.* **93,** 673 (1984).
10. Louwers, S. P. A., and Prins, R., *J. Catal.* **139,** 525 (1993).
11. Pollack, S. S., Makovsky, L. E., and Brown, F. R., *J. Catal.* **59,** 452 (1979).
12. Gachet, C., Paulus, R., de Mourgues, L., Durand, C., and Toulhoat, H., *Bull. Soc. Chim. Belg.* **93,** 681 (1984).
13. Sørensen, O., Clausen, B. S., Candia, R., and Topsøe, H., *Appl. Catal.* **13,** 363 (1985).
14. Pratt, K. C., Sanders, J. V., and Christov, V., *J. Catal.* **124,** 416 (1990).
15. Srinivasan, S., Datye, A. K., and Peden, C. H. F., *J. Catal.* **137,** 513 (1992).
16. Blanchard, L., Grimblot, J., and Bonnelle, J. P., *J. Catal.* **98,** 229 (1986).
17. Sanders, J. V., and Pratt, K. C., *J. Catal.* **67,** 331 (1981).
18. Houssenbay, S., Kasztelan, S., Toulhoat, H., Bonnelle, J. P., and Grimblot, J., *J. Phys. Chem.* **93,** 7176 (1989).
19. Ramachandran, R., and Massoth, F. E., *J. Catal.* **67,** 248 (1981).
20. Kasztelan, S., Toulhoat, H., Grimblot, J., and Bonnelle, J. P., *Appl. Catal.* **13,** 127 (1984).
21. Topsøe, H., and Clausen, B. S., *Appl. Catal.* **25,** 273 (1986).
22. Prins, R., de Beer, V. H. J., and Somorjai, G. A., *Catal. Rev.-Sci. Eng.* **31,** 1 (1989).
23. Bouwens, S. M. A. M., van Veen, J. A. R., Koningsberger, D. C., de Beer, V. H. J., and Prins, R., *J. Phys. Chem.* **95,** 123 (1991).
24. Louwers, S. P. A., and Prins, R., *J. Catal.* **133,** 94 (1992).
25. Garreau, F. B., Toulhoat, H., Kasztelan, S., and Paulus, R., *Polyhedron* **5,** 211 (1986).
26. Delmon, B., *in* "Catalysts in Petroleum Refining 1989" (D. L. Trimm *et al.*, Eds.), p. 1. Elsevier, Amsterdam, 1990.
27. Tanaka, K.-I., and Okuhara, T., *Catal. Rev.-Sci. Eng.* **15,** 24 (1977).
28. Okamoto, Y., Tomioka, H., Imanaka, T., and Teranishi, S., *J. Catal.* **66,** 93 (1980).
29. Wambeke, A., Jalowiecki, L., Kasztelan, S., Grimblot, J., and Bonnelle, J. P., *J. Catal.* **109,** 320 (1988).
30. Karroua, M., Grange, P., and Delmon, B., *Appl. Catal.* **50,** L5 (1989).
31. Karroua, M., Matralis, H., Grange, P., and Delmon, B., *J. Catal.* **139,** 371 (1993).
32. Farragher, A. L., and Cossee, P., *in* "Proceedings, 5th Int. Congress Catalysis, Palm Beach, 1972" (J. W. Hightower, Ed.), p. 1301. North Holland, Amsterdam, 1973.